American Mineralogist, Volume 89, pages 164–175, 2004

A computational investigation of the Al/Fe/Mg order-disorder behavior in the dioctahedral sheet of phyllosilicates

ERIKA J. PALIN,[1,*] MARTIN T. DOVE,[1] ALFONSO HERNÁNDEZ-LAGUNA,[2] AND C. IGNACIO SAINZ-DÍAZ[2]

[1]Department of Earth Sciences, University of Cambridge, Downing Street, Cambridge CB2 3EQ, U.K.
[2]Departamento de Ciencias de la Tierra y Química Ambiental, Estación Experimental del Zaidín (CSIC), C/ Profesor Albareda, 1, 18008-Granada, Spain

ABSTRACT

In previous papers, we investigated via Monte Carlo simulation the order-disorder behavior of an individual octahedral phyllosilicate sheet, with respect to two-species systems Al/Fe, Al/Mg, and Fe/Mg, and some three-species systems Al/Fe/Mg that were relevant to clay compositions found in nature. We have extended the work on Al/Fe/Mg systems to include a wide range of different octahedral compositions that can represent different natural and synthetic clay minerals, by means of Monte Carlo simulations based only on atomistic models. In many cases, phase transitions do not occur, in that long-range order is not attained, but most systems exhibit short-range order at low temperatures. The ordering of the octahedral cations is highly dependent on the cation composition.

INTRODUCTION

Phyllosilicates are chemically versatile minerals that are able to undergo a wide variety of cation substitutions to produce large numbers of different minerals. Many of the possible substitutions relate to the sheet of octahedrally coordinated cations that is present in almost all phyllosilicates. Such octahedral sheets can be either dioctahedral, in which 2/3 of the sites are occupied by cations, or trioctahedral, in which all sites are occupied. Our interest so far has been in the dioctahedral sheets, found in minerals such as muscovite, paragonite, kaolinite, and montmorillonite. These sheets can accommodate many different cation species, with those most commonly found being Al^{3+}, Fe^{3+}, and Mg^{2+}.

Experiments on phyllosilicates have yielded many and varied results for the configuration of the octahedral sheets, particularly in natural samples of 2:1 phyllosilicates. An ordered distribution of octahedral cations was found in celadonites where the Al^{3+} and Fe^{3+} ions tend to segregate from each other (Besson et al. 1987). Drits et al. (1997) found a certain short-range ordering in the octahedral sheet in celadonite, glauconite, and Fe-illite by using IR, Mössbauer, and EXAFS spectroscopies. Schroeder (1993) found by means of ^{27}Al NMR that Fe mixes with Al in shale illite-smectite (I-S) samples with low Fe content but Fe segregates from Al in Fe-rich specimens. Muller et al. (1997) observed that Mg and Fe form clusters that segregate from Al in the Camp-Bertaux montmorillonite by using XRD, EXAFS, and FTIR. In some synthetic smectite samples, Grauby et al. (1991) found that Al^{3+} and Fe^{3+} tend to mix rather than to segregate, Mg^{2+} and Fe^{3+} segregate within the same layer, and Mg^{2+} and Al^{3+} segregate creating dioctahedral and trioctahedral layers. FTIR and ^{27}Al NMR spectroscopic studies and Reverse Monte Carlo (RMC) simulations on illite/smectite samples showed short-range ordering of the octahedral cations with a tendency to be segregated for Fe^{3+} cations and dispersed for Mg^{2+} cations (Cuadros et al. 1999; Sainz-Díaz et al. 2001a). Therefore, these different results make it difficult to extract a definitive conclusion from experimental studies.

In previous papers, we investigated the order-disorder behavior of the tetrahedral sheet (Al/Si) in muscovite (Palin et al. 2001); the tetrahedral (Al/Si) and octahedral (Al/Mg) sheets in phengite (Palin et al. 2003); and the octahedral sheet in illites and smectites, both with respect to two-species systems Al/Fe, Al/Mg, Fe/Mg and to some three-species systems Al/Fe/Mg with compositions relevant to naturally occurring clay minerals (Sainz-Díaz et al. 2003a, 2003b).

In this work, we extend our sampling of Al/Fe/Mg compositions to include many more across the possible phase space. These new compositions are not necessarily relevant to natural samples, but nevertheless they may be of interest in the field of clay mineral synthesis.

We have used our own Monte Carlo program, Ossia, to investigate the behavior of the octahedral sheet with these different compositions. By doing so, we have determined that the observed behavior is very sensitive to changes in composition, and we present below some examples of different behavior in a variety of different systems.

METHOD

We have developed a consistent approach to simulation studies of cation ordering, which is described in detail elsewhere (Bosenick et al. 2001; Warren et al. 2001). The approach consists of two stages. The first stage is to use the program GULP (Gale 1997) with empirical interatomic potentials and lattice energy minimization methods to compute values for the cation exchange interaction parameters (which are labeled *J*). The basic interatomic potential model has previously been used to reproduce accurately structures and crystal properties of 2:1 phyllosilicates, especially smectites and illites (Sainz-Díaz et al. 2001b). Details

* E-mail: ejp24@cam.ac.uk

of the potentials used, and values for the parameters therein, are given in Appendix 1.

Once the exchange interaction parameters have been determined, the second stage of the approach is the use of these parameters in Monte Carlo simulations of ordering as a function of temperature.

A detailed discussion of the determination of the exchange interaction parameters for the octahedral sheet with respect to two-species systems has been given in previous papers (Sainz-Díaz et al. 2003a, 2003b). Here we merely quote the values of the interaction parameters for two-species systems (Table 1) and explain how, once these values are known, it is possible to extend the formalism for the case of a three-species system.

For a system with two ordering species, A and B, we can write the energy of the system as

$$E = E_0 + \sum_n N^n_{\mathrm{A-A}} J_n \tag{1}$$

where $J_n = E_{\mathrm{A-A}} + E_{\mathrm{B-B}} - 2E_{\mathrm{A-B}}$, $N^n_{\mathrm{A-A}}$ is the number of A–A interactions over a distance corresponding to a particular J_n, and E_0 is a constant term that is not involved in the ordering process. There are no terms dependent on B atoms, since these are wholly determined by those dependent on A atoms.

If similar analysis is performed for a system with A and C cations, and a system with B and C cations, then the J formalism can be extended to the case of three ordering species, A, B, and C. Specifically, the pair energies for the two-cation systems are

$$\begin{aligned} J^{(AB)} &= E_{\mathrm{A-A}} + E_{\mathrm{B-B}} - 2E_{\mathrm{A-B}} \\ J^{(AC)} &= E_{\mathrm{A-A}} + E_{\mathrm{C-C}} - 2E_{\mathrm{A-C}} \\ J^{(BC)} &= E_{\mathrm{B-B}} + E_{\mathrm{C-C}} - 2E_{\mathrm{B-C}} \end{aligned} \tag{2}$$

It can be shown (Bosenick et al. 2001) that for three cation types, the energy becomes

$$E = E_0' + \sum_n N^n_{\mathrm{A-A}} J^n_{\mathrm{A-A}} + N^n_{\mathrm{B-B}} J^n_{\mathrm{B-B}} + N^n_{\mathrm{C-C}} J^n_{\mathrm{C-C}} \tag{3}$$

where E_0' is another constant term (different from E_0 in Eq. 1), and the J values $J^n_{\mathrm{A-A}}$ etc are given by

$$\begin{aligned} J_{\mathrm{A-A}} &= \frac{1}{2}[J^{(AB)} + J^{(AC)} - J^{(BC)}] \\ J_{\mathrm{B-B}} &= \frac{1}{2}[J^{(AB)} + J^{(BC)} - J^{(AC)}] \\ J_{\mathrm{C-C}} &= \frac{1}{2}[J^{(AC)} + J^{(BC)} - J^{(AB)}] \end{aligned} \tag{4}$$

where the $J^{(AB)}$ etc are given in Equation 2. Hence, with J values for the systems Al/Fe, Al/Mg, and Fe/Mg, we can calculate values for the three-species system Al/Fe/Mg (Table 2).

TABLE 1. Exchange interaction (J) values determined for two-species systems Al/Mg, Al/Fe, and Fe/Mg

System	J_1 (eV)	J_2 (eV)	J_3 (eV)	J_4 (eV)
Al/Mg	0.656 (16)*	0.168(14)*	0.089 (18)*	0.025 (8)*
	0.652 (14)†	0.162 (10)†	0.088 (10)†	0.015 (9)†
	0.620 (18)‡	0.151 (11)‡	0.066 (12)‡	0.030 (9)‡
Al/Fe	0.025 (2)§	0.007 (1)§	0.003 (1)§	0.003 (1)§
	0.015 (3) ||	0.005 (2) ||	0.008 (3) ||	0.001 (2) ||
Fe/Mg	0.456 (31)#	0.101 (23)#	–0.003 (27)#	0.075 (20)#

* Obtained from $K_{1.28}(Si_{7.72}Al_{0.28})(Al_3Mg)(OH)_4O_{20}$ as unit cell.
† From $Na_{1.28}(Si_{7.72}Al_{0.28})(Al_3Mg)(OH)_4O_{20}$.
‡ From $K_{1.8}(Si_{7.2}Al_{0.8})(Al_3Mg)(OH)_4O_{20}$.
§ From $K_{0.28}(Si_{7.72}Al_{0.28})(Al_3Fe)(OH)_4O_{20}$.
|| From $K_{0.8}(Si_{7.2}Al_{0.8})(Al_3Fe)(OH)_4O_{20}$.
From $K_{2.28}(Si_{7.72}Al_{0.28})(Fe_2Mg_2)(OH)_4O_{20}$.

TABLE 2. Exchange interaction (J) values determined for three-species systems Al/Fe/Mg

	J_1 (eV)	J_2 (eV)	J_3 (eV)	J_4 (eV)
Al-Al	0.105	0.033	0.049	–0.029
Fe-Fe	–0.085	–0.027	–0.044	0.031
Mg-Mg	0.545	0.127	0.041	0.049

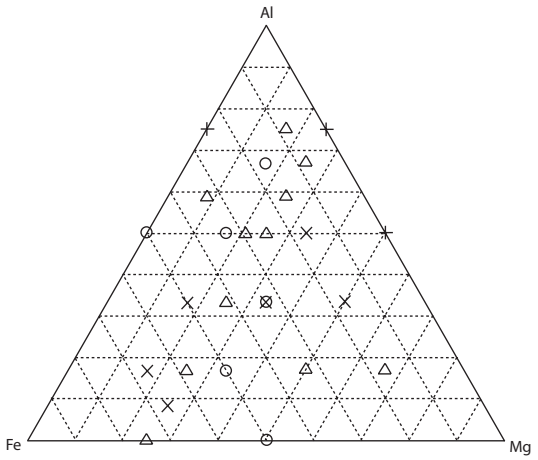

FIGURE 1. Ternary phase diagram showing octahedral sheet compositions studied. × indicates compositions discussed in this work. + indicates compositions studied in Sainz-Díaz et al. (2003a). Circle indicates compositions discussed in Sainz-Díaz et al. (2003b). Triangle indicates remaining compositions studied, for which data are available on the internet at http://www.esc.cam.ac.uk/minsci/downloads/3specmc.

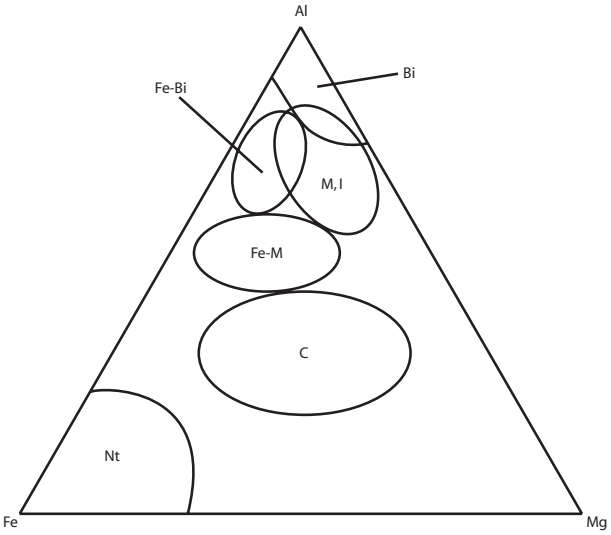

FIGURE 2. Ternary phase diagram showing the range of naturally occurring illite and smectite minerals (after Güven 1988). Bi = beidellites; Fe-Bi = Fe-rich beidellites; M, I = montmorillonites, illites; Fe-M = Fe-rich montmorillonites; C = celadonites; Nt = nontronites.

Simulation details

We performed the Monte Carlo simulations for a single octahedral sheet with 1296 sites. Simulations were each run at twenty different temperatures, and in some cases, subsequent simulations were run over smaller temperature ranges to examine behavior near possible phase transitions.

The MC algorithm is a standard Metropolis algorithm; at each MC step, two atoms are selected at random and swapped, and the energies before and after the swap are compared. If the energy decreases, the swapped configuration is retained and the next MC step follows; if the energy increases, however, the swapped configuration is retained only subject to the following probability test:

$$P(E \rightarrow E + \Delta E) = \exp\left(\frac{-\Delta E}{k_B T}\right) \quad (5)$$

This test also controls the temperature of the simulation, since the value of its outcome will depend on the Boltzmann factor, which causes the various possible atomic configurations to occur with different probabilities at different temperatures. Each simulation consists of two parts, an equilibration component and a production component. Each of these consists of the same number of steps. The equilibration stage is designed to allow the system to relax to equilibrium before the thermodynamic quantities are calculated in the production stage. Averages of these properties are taken every 500 MC steps in the production component. Typically, simulations are carried out for around 10^8 steps (that is, 10^8 steps for each of the equilibration and production runs). In this study we used 200 million steps.

All simulations were performed by starting the system in an initially random configuration, since we were not able to postulate ordered structures from which to begin. At the end of each simulation, the thermodynamic quantities $\langle E \rangle$ and $\langle E^2 \rangle$ are output, from which the heat capacity C of the system can be calculated:

$$C = \frac{\langle E^2 \rangle - \langle E \rangle^2}{k_B T^2} \quad (6)$$

In the case of a second-order phase transition, the heat capacity will diverge at T_c and hence is a useful measure of any ordering phase transitions that may occur. It is especially useful for us in these simulations, since it is difficult to measure phase transitions using order parameters when the ordering schemes observed can be very complicated.

Several Al/Fe/Mg mixtures were studied representing different octahedral

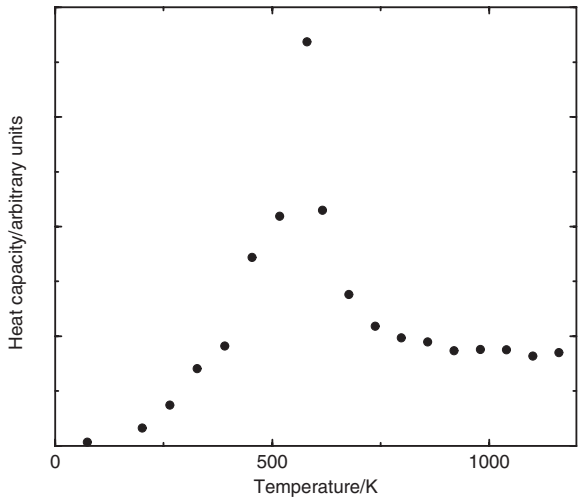

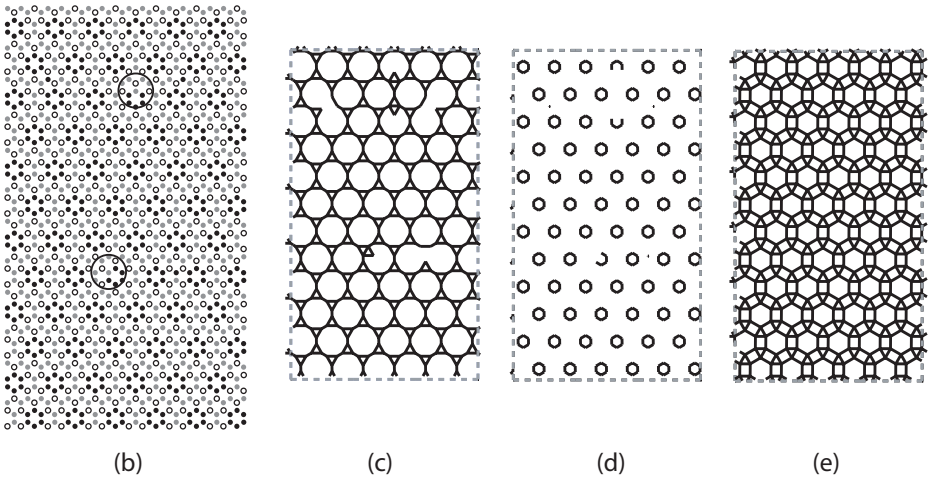

FIGURE 3. Results for Al/Fe/Mg = 1/1/1. (**a**) Variation of heat capacity with temperature. (**b**) Structural snapshot at low temperature; grey circles indicating Al, black circles Fe, and open circles Mg. Selected defects in the ordering pattern are ringed. (**c**) Plot of Al cations only, showing linkages up to J_2. (**d**) Plot of Fe cations only, showing J_1 linkages. (**e**) Plot of Mg cations only, showing linkages up to J_3.

cation compositions of 2:1 phyllosilicates. Previously, we studied the compositions (Al/Fe/Mg): 1/1/1, 1/3/2, 3/2/1, and 4/1/1, as they are relevant to natural phyllosilicates. In this work we have extended the study by covering a wide range of compositions for the ternary system Al/Fe/Mg. Samples with a high Al content have been selected, such as 7/4/1, 7/2/3, 12/7/5, 2/1/1, and 3/1/2. These compositions represent octahedral compositions of some natural dioctahedral 2:1 phyllosilicates. The samples 7/2/3 and 3/1/2 can be included in the smectite-illite group, although the Mg content in 3/1/2 is high. The samples 7/4/1, 12/7/5, and 2/1/1 can be included in the Fe-rich-montmorillonite group (Güven 1988). Samples with a high Fe content (1/4/1, 1/8/3, and 2/7/3), Mg-rich samples (1/2/3 and 1/1/4), and samples with similar compositions of each cation (2/3/1, 4/5/3, and 2/1/3) were also selected. Samples 1/4/1 and 1/8/3 can represent natural nontronites and 2/7/3

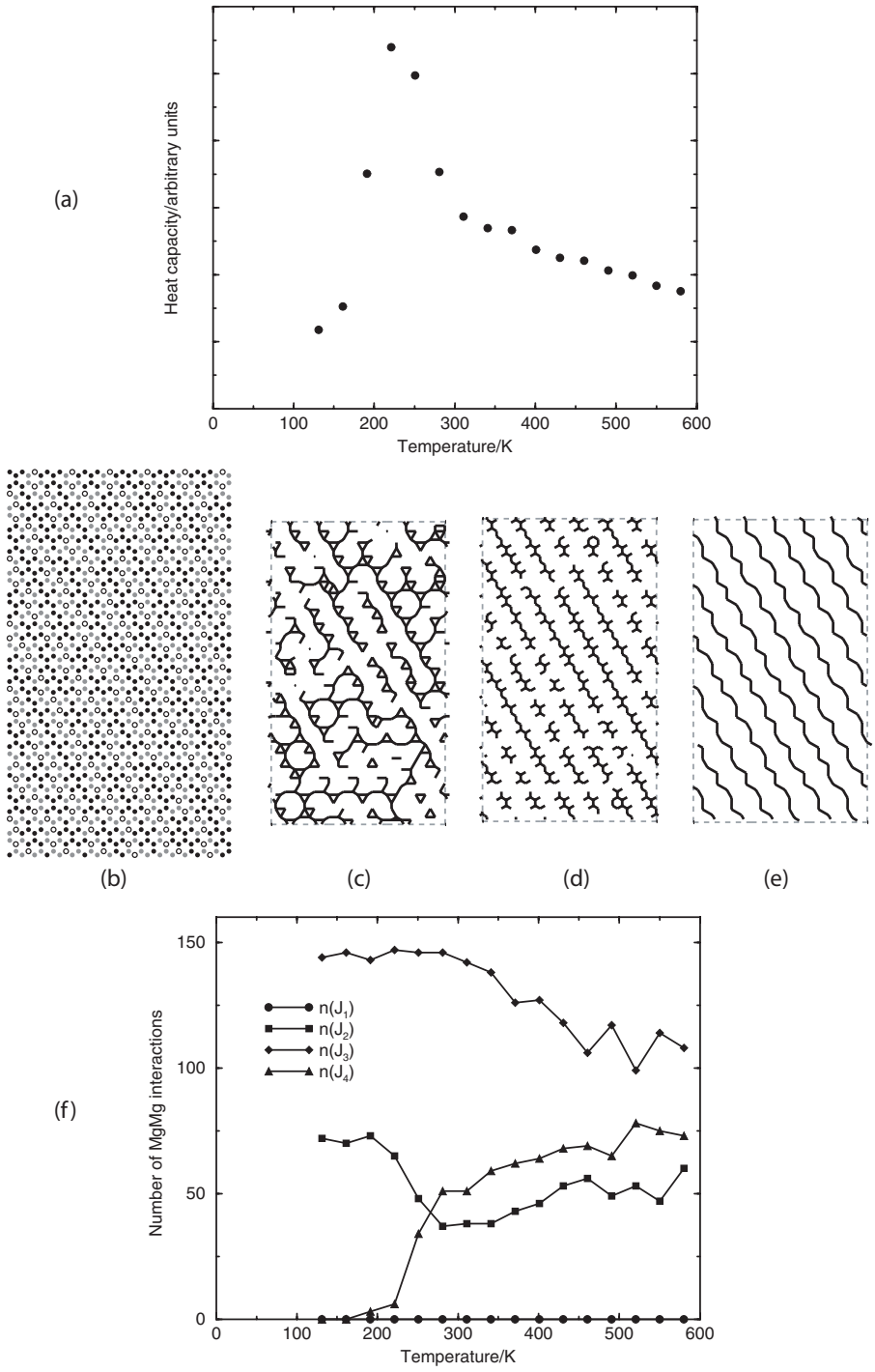

FIGURE 4. Results for Al/Fe/Mg = 2/3/1. (**a**) Heat capacity data at various temperatures. (**b**) Snapshot of structure at low temperature. Grey circles indicate Al, black circles Fe, and open circles Mg. (**c**) Plot of Al cations only, showing linkages up to J_2. (**d**) Plot of Fe cations only, showing J_1 linkages. (**e**) Plot of Mg cations only, showing linkages up to J_3. (**f**) Plot of $nJ_{n,\mathrm{Mg–Mg}}$.

can be a nontronite with a high Mg content (Güven 1988). Samples 2/3/1 and 4/5/3 can represent natural celadonites (Güven 1988). Samples 1/2/3, 1/1/4, and 2/1/3 are less likely to be found in nature, since they have a high Mg content and this composition tends to form a trioctahedral domain rather than a dioctahedral one. Nevertheless, all samples can also represent different synthetic clay samples that can be found by experiment.

These compositions are plotted on a ternary phase diagram in Figure 1 to illustrate the coverage of phase space. Also plotted are the compositions of the binary systems and ternary systems that were studied previously (Sainz-Díaz et al. 2003a, 2003b). Figure 2 shows a similar plot illustrating the octahedral sheet compositions that have been found in naturally occurring smectite and illite minerals (Güven 1988). Comparing Figures 1 and 2, one can observe that we have studied some compositions that are difficult to find in nature. However, they are very interesting in the context of experimental work on synthetic clay minerals.

RESULTS

Due to the volume of data generated in the course of this work, we have chosen to give results here only for selected compositions. We have also included the 1/1/1 sample reported previously (Sainz-Díaz et al. 2003b), since it has no composition preference for any cation and can be a good reference for comparison purposes. Some samples of each type have been selected to highlight the effect of the cation composition on the ordering. The full sets of results are available on the internet at http://www.esc.cam.ac.uk/minsci/downloads/3specmc.

For each of the compositions discussed in detail below, the lowest-energy configuration is given, since this is statistically the structure that will be the most ordered. The lowest-energy configuration is not necessarily that corresponding to the lowest temperature, since the results of our MC simulations at low temperature are often poorly equilibrated. For each of the lowest-energy configurations, plots are also shown of the individual Al, Fe, and Mg cation networks. In these figures, Al atoms are linked together over J_1 and J_2 distances, Fe atoms over J_1 distances, and Mg over J_1, J_2, and J_3 distances. We refer to these figures as

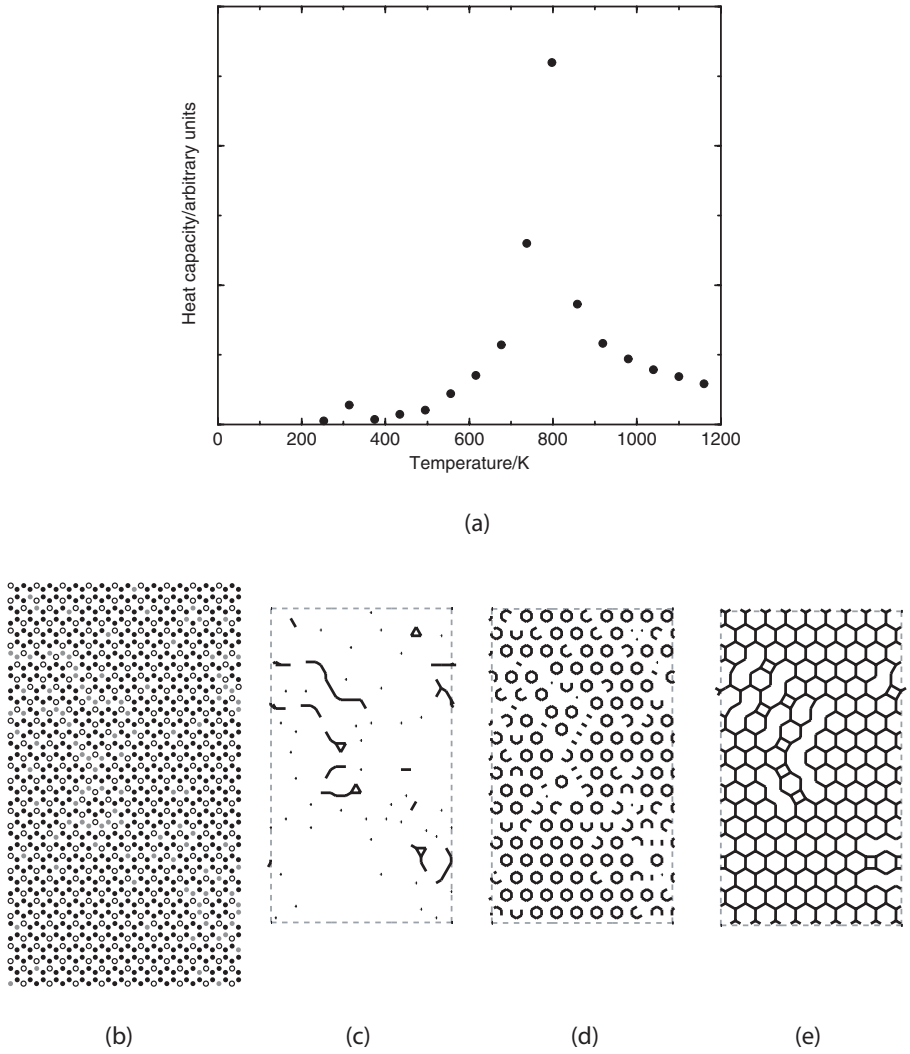

FIGURE 5. Results for Al/Fe/Mg = 1/8/3. (**a**) Plot of heat capacity as a function of temperature. (**b**) Low-temperature snapshot of structure. Grey circles indicate Al, black circles Fe, and open circles Mg. (**c**) Partial ordering pattern for Al. (**d**) Partial ordering pattern for Fe. (**e**) Partial ordering pattern for Mg.

"partial ordering patterns."

We also give data for the heat capacity in each system. We have determined that even for systems without perfect long-range order, there are often anomalies in the heat capacity at a certain temperature, and that sharper anomalies tend to correspond to better ordering. In our simulations, we compute at each temperature the number of linkages of each type (J_1, J_2, etc.) for each type of atom (Al, Fe, Mg). Plots of these parameters, $nJ_{n,i-i}$, as a function of temperature are sometimes useful in examining ordering processes.

Al/Fe/Mg = 1/1/1

Dioctahedral phyllosilicates with this composition can be included as members of the celadonite group. Although it has been discussed in our previous paper (Sainz-Díaz et al. 2003b), we reiterate it here, since it is the simplest three-species composition. The system undergoes a phase transition at approximately 580 K (as evidenced by the heat capacity anomaly shown in Fig. 3a) to produce the ordered structure shown in Figure 3b. Figures 3c–3e show partial ordering patterns for Al, Fe, and Mg atoms respectively. The order is almost perfect; only a few cations are erroneously placed, and two of these are marked with circles on Figure 3b.

In the ordered configuration of this model, there are no Mg-Mg nearest-neighbor pairs, according to the experimental behavior of Mg^{2+} in octahedral sheet of smectites, illites (Sainz-Díaz et al. 2001a), and nontronites (Manceau et al. 2000). Furthermore, the Fe^{3+} cations segregate in small globular clusters. This is consistent with experimental results that found a clustering tendency of Fe^{3+} in natural smectites and illites from IR, NMR spectroscopy, and RMC simulations (Sainz-Díaz et al. 2001a), and in nontronites (Manceau et al. 2000), where small Fe domains separated by Al and Mg cations were found. This fact is also in agreement with the lack of magnetic ordering observed in these minerals at low temperatures (Lear and Stucki 1990).

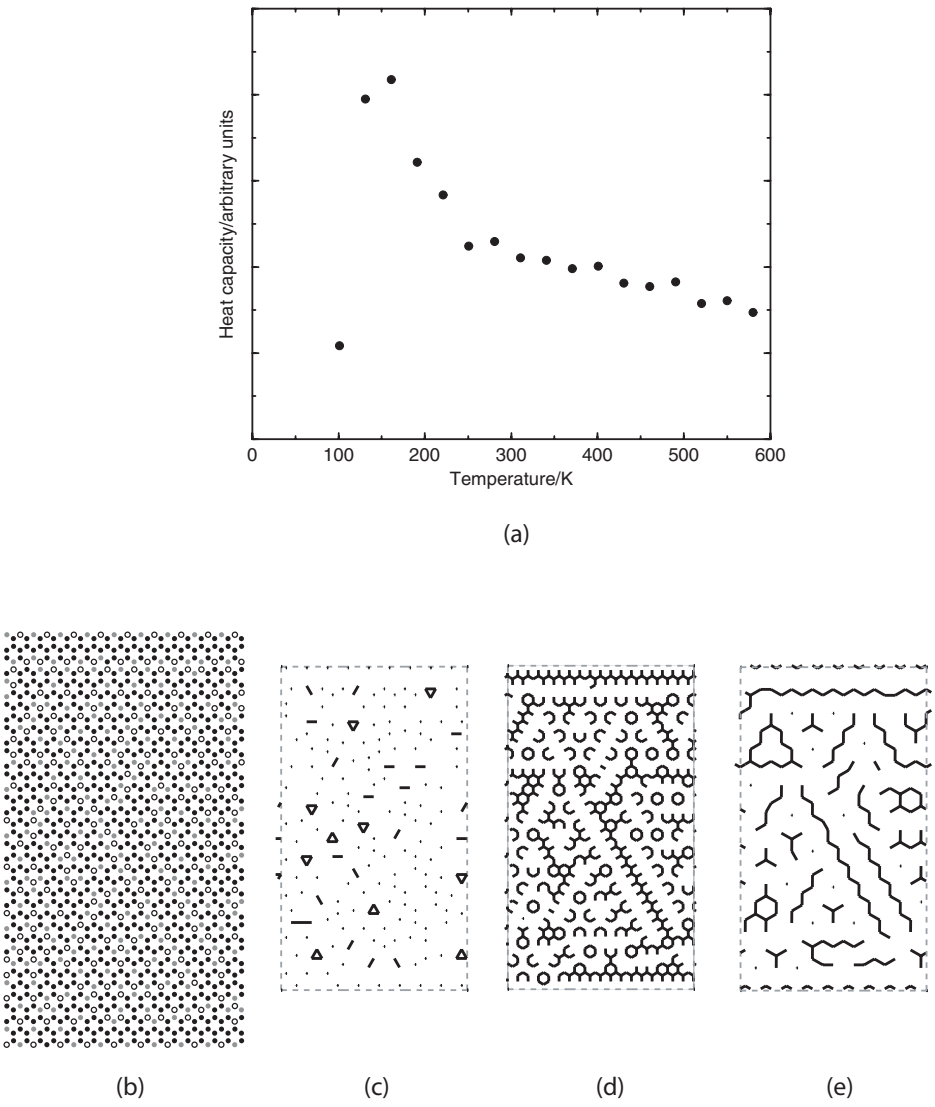

FIGURE 6. Results for Al/Fe/Mg = 1/4/1. (**a**) Heat capacity data. (**b**) Low-temperature structure snapshot. Grey circles indicate Al, black circles Fe, and open circles Mg. (**c**) Partial ordering pattern for Al. (**d**) Partial ordering pattern for Fe. (**e**) Partial ordering pattern for Mg.

Al/Fe/Mg = 2/3/1

As with the previous sample, we can include this composition in the celadonite group. The heat capacity data for the 2/3/1 system in Figure 4a suggest that a phase transition occurs at ~230 K. However, the pattern formed as a result of this transition is not perfectly long-range-ordered; it is shown in Figure 4b. We can describe this system as long-range-ordered with defects. The Fe network is controlled mainly by J_1 interactions, whereas the Mg network is controlled mainly by J_3 interactions. The Fe and Mg networks (Figs. 4d and 4e) show a good attempt at long-range ordering, in spite of the defects. A plot of $nJ_{n,\mathrm{Mg-Mg}}$ (Fig. 4f) shows that nearest-neighbor Mg–Mg interactions are avoided, with a sudden increase in the number of J_2 linkages and decrease in the number of J_4 linkages at T_c. In this case the Fe cations form linear chains with interruptions in the ordered configurations. This ordering is clearly different from that in the previous case.

Al/Fe/Mg = 1/8/3

This model can represent the composition of some natu-

ral nontronites. In this system, the profile of the heat capacity graph (Fig. 5a) suggests a phase transition at around 810 K. Once again, however, perfect long-range order is not attained, although most regions of the structure are ordered. The structure in this system (Fig. 5b) consists mainly of Mg atoms linked by J_3 interactions forming a "superhexagon" pattern—that is, a hexagonal pattern that is larger than the pattern formed by one hexagonal ring in the structure. This pattern is illustrated more clearly in the separate partial ordering patterns for Fe and Mg (Figs. 5d and 5e). The presence of a small amount of Al produces faults in this pattern, which can be seen most clearly in Figure 5e. The Al partial ordering pattern in Figure 5c shows that isolated Al atoms disrupt the ordering less than do grouped Al atoms. In fact, a configuration with perfect Mg order was obtained at a different temperature, but had a higher energy than the configuration shown in the figure (–0.0677 eV/atom, compared with –0.0686 eV/atom).

In other systems we have studied, including the tetrahedral sheet in muscovite (Palin et al. 2001) and some of the octahedral sheets with two-species occupancy (Sainz-Díaz et al. 2003a, 2003b), a species ratio of 3:1 leads to the production of the "superhexagon" pattern. From the results for this Al/Fe/Mg composition, we might infer that the likely behavior of this system would be to produce the superhexagon pattern as well, since the composition Al/Fe/Mg = 1/8/3 is not far from Fe/Mg = 3/1 on the ternary diagram (Fig. 1). We performed a simulation of this two-species composition, and the superhexagon pattern did indeed form, at a T_c of ~930 K.

The ordering pattern of Fe in the most stable ordered configuration of this sample is similar to that found in the Al/Fe/Mg = 1/1/1 model, where the Fe cations form isolated globular clusters with some defects in the long-range ordering, in accordance with experimental results (Manceau et al. 2000). Similar behavior was found in the Al/Fe/Mg = 2/7/3 sample.

Al/Fe/Mg = 1/4/1

The composition Al/Fe/Mg = 1/4/1 is within the nontronite region of the phase diagram (Fig. 1). The heat capacity data in Figure 6a show an anomaly, although it is difficult to tell from the data whether or not this is a true phase transition. However, the low-temperature structure of the system shown in Figure 6b, together with the network plots for Al, Fe, and Mg in Figures 6c–e, suggest that there is a fairly high degree of order. The behavior of this system has elements of that found in other samples with similar compositions; in some regions, the Fe atoms form chains (similar behavior to that in the 2/3/1 system), and in others they form clusters (similar behavior to the 1/8/3 and Fe/Mg = 3/1 systems). The formation of chains could have implications for the magnetic properties of such minerals.

Al/Fe/Mg = 2/1/3

Although this composition is not commonly found in the natural dioctahedral 2:1 phyllosilicates, it has been included as an example of an Mg-rich sample to study the effect of cation content on the cation ordering. In this sample, a phase transition occurs at approximately 1740 K (Fig. 7a). In the ordered structure

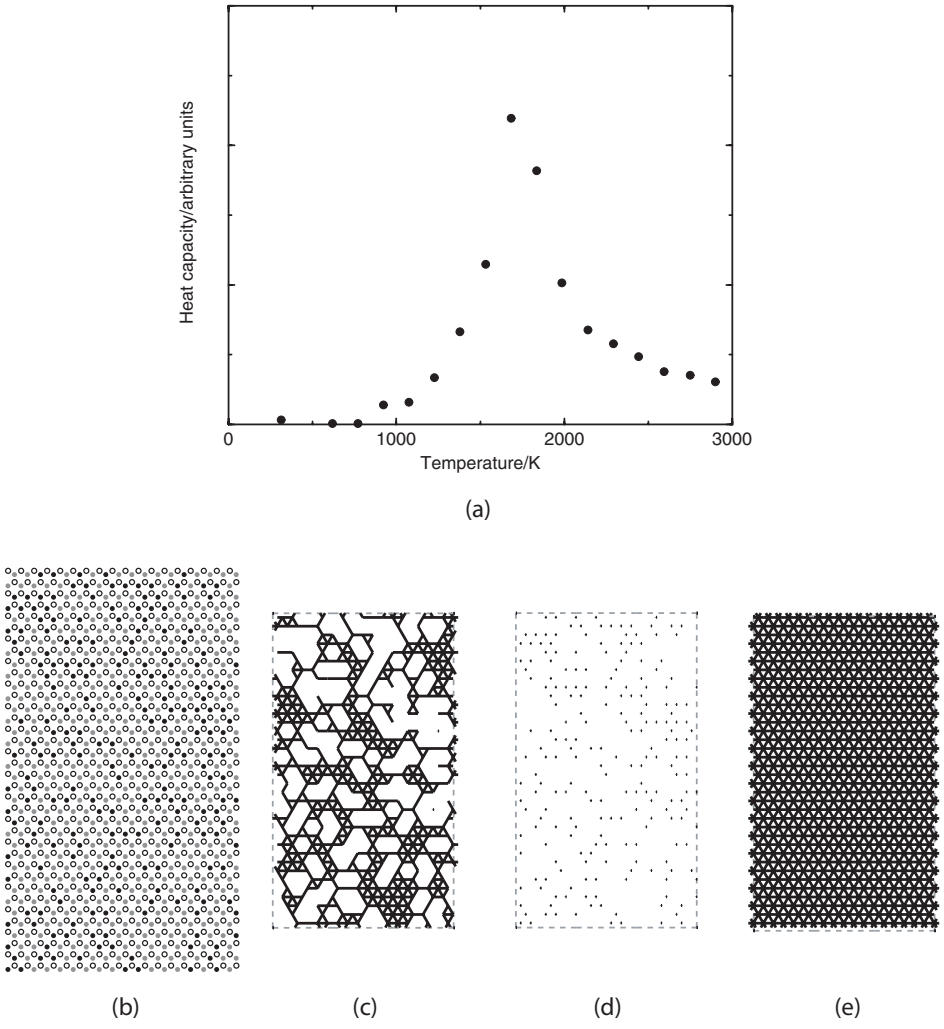

FIGURE 7. Results for Al/Fe/Mg = 2/1/3. (**a**) Data for heat capacity. (**b**) Structure snapshot at low temperature. Grey circles indicate Al, black circles Fe, and open circles Mg. (**c**) Partial ordering pattern for Al. (**d**) Partial ordering pattern for Fe. (**e**) Partial ordering pattern for Mg.

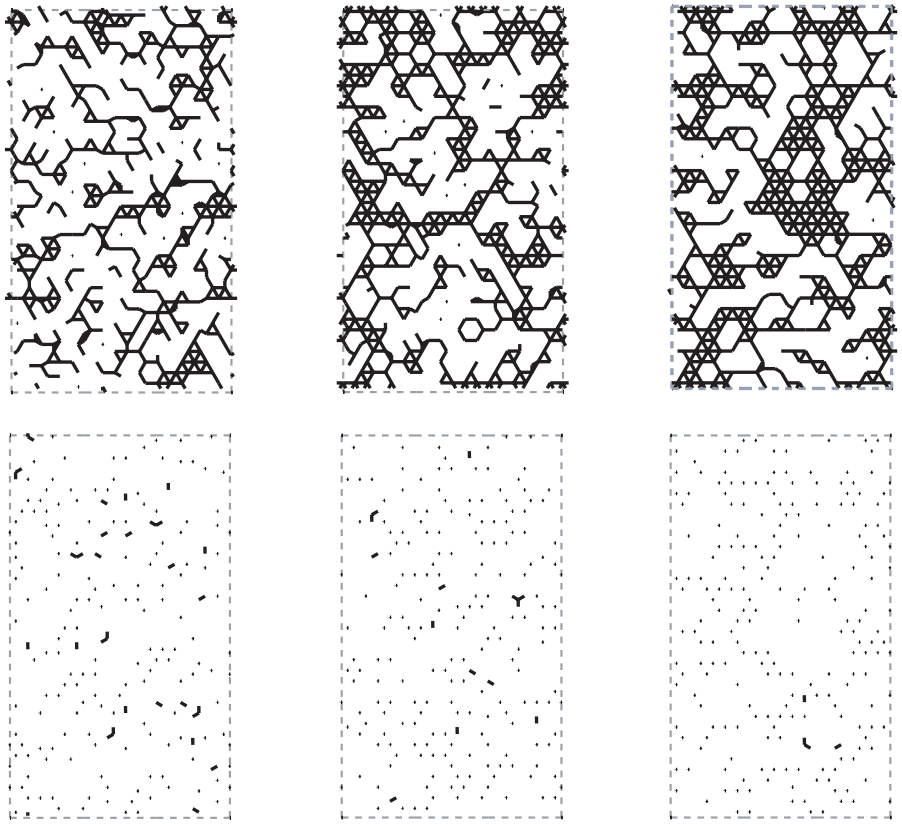

(a)

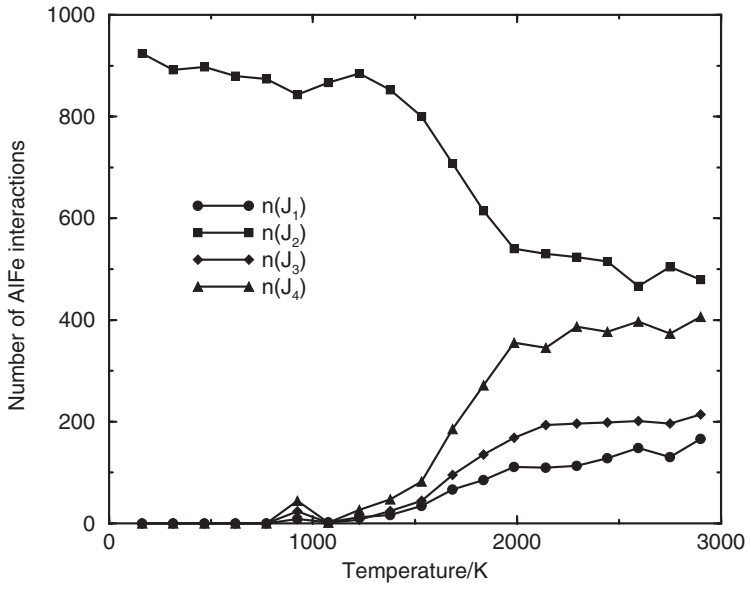

(b)

FIGURE 8. Al/Fe/Mg = 2/1/3: (**a**) partial ordering patterns for Al (top) and Fe (bottom) at $T >> T_c$ (left), $T \sim T_c$ (middle), and $T < T_c$ (right). (**b**) Plot of $nJ_{n,\text{Al–Fe}}$ indicating separation of Al and Fe as T decreases.

(Fig. 7b), the Mg atoms are long-range ordered, with all Mg-Mg linkages as J_2. The Al and Fe linkages are also all J_2 (Figs. 7c and 7d—note that in the Fe network there are no linkages, since Fe atoms are only linked to J_1 distances in these plots). Essentially, then, the 2/1/3 system can be viewed as a 2:1 mixture of Al/Mg 1/1 and Fe/Mg 1/1 ordered phases. Furthermore, examination of the behavior near the phase transition indicates that both these components form cooperatively, rather than each one forming at its own T_c (1600 K for Al/Mg 1/1 and 1880 K for Fe/Mg 1/1—Sainz-Díaz et al. 2003a, 2003b). This is illustrated in Figure 8a, which shows Al and Fe network plots (Mg plots not shown) for selected temperatures. Additionally, a plot of the number of Al–Fe linkages (Fig. 8b) shows that the number of J_2 linkages increases with decreasing temperature, but the other linkages decrease; this is consistent with the separation of Al and Fe into different regions. Hence, no clustering of Fe is found in samples with this composition. Similar ordering behavior was found in samples with Al/Fe/Mg = 1/2/3 and 1/1/4. A high Mg content inhibits the formation of Fe clusters. This behavior was not found experimentally, because this composition is more likely in trioctahedral phyllosilicates and no natural dioctahedral clay minerals have been reported with this composition.

Al/Fe/Mg = 3/1/2

This composition is close to smectites with high Mg content. In this system, there is once again an anomaly in the heat capacity plot (Fig. 9a) without the occurrence of long-range order, although we believe there is still sufficient order to call this a phase transition. The lowest-energy structure is shown in Figure 9b, together with the individual partial ordering patterns in Figures 9c–9e.

The system is quite complex. There are attempts at ordering in the same pattern as that found in the 1/1/1 system, which can be seen in all three of the partial ordering patterns. The remaining areas are predominantly an Al/Mg phase—examination of the partial ordering patterns reveals that in areas of high Al and Mg concentration, there is little or no Fe. This Al/Mg phase is not long-range-ordered, but there is some evidence for short-range order; for example, the Mg atoms avoid forming J_1 linkages. The

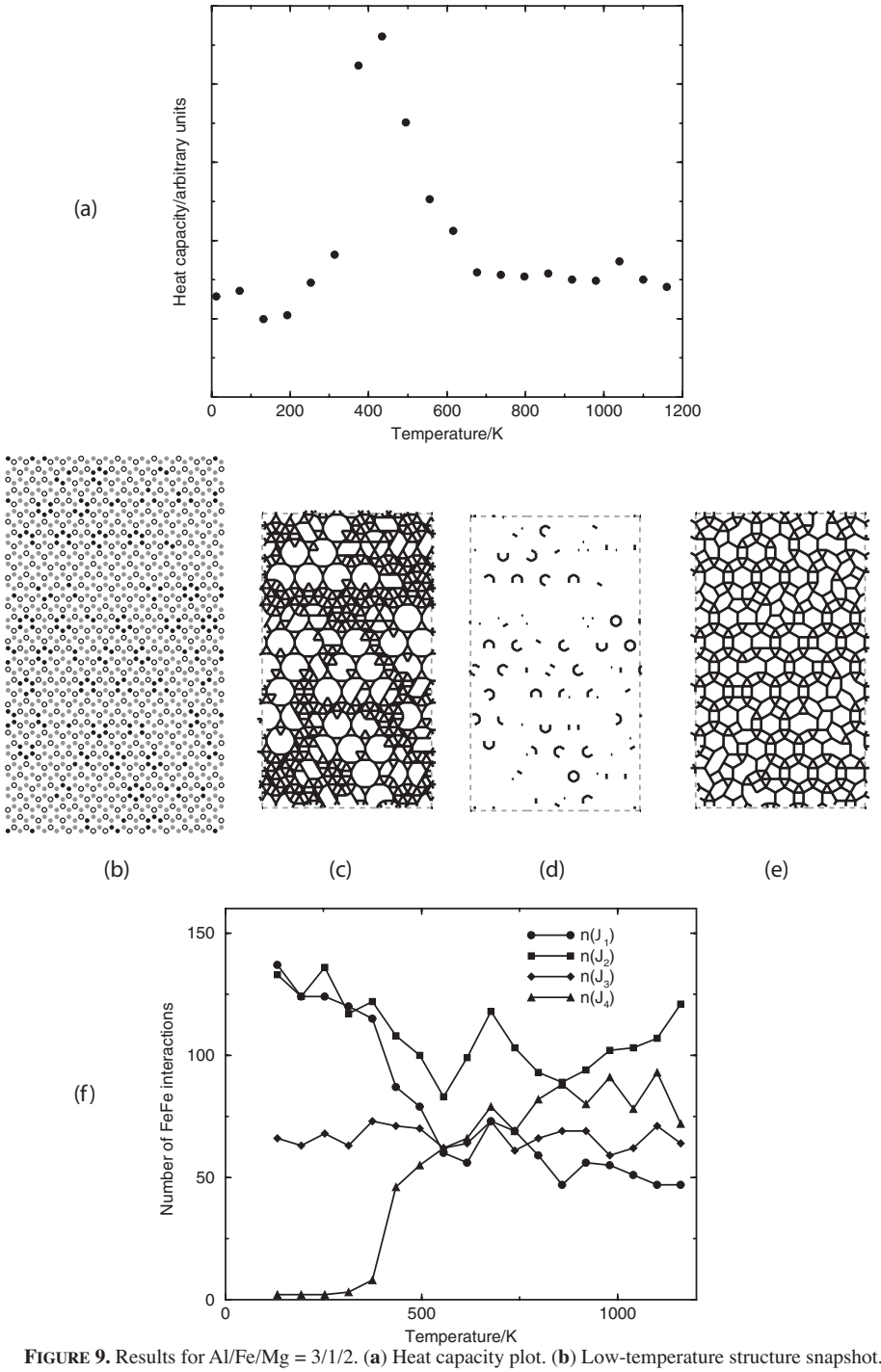

FIGURE 9. Results for Al/Fe/Mg = 3/1/2. (**a**) Heat capacity plot. (**b**) Low-temperature structure snapshot. Grey circles indicate Al, black circles Fe, and open circles Mg. (**c**) Partial ordering pattern for Al. (**d**) Partial ordering pattern for Fe. (**e**) Partial ordering pattern for Mg. (**f**) Plot of $nJ_{n,\mathrm{Fe–Fe}}$.

clustering of the Fe atoms at low temperature can be observed from the $nJ_{n,\mathrm{Fe-Fe}}$ plot in Figure 9f. As the temperature decreases, the number of J_1 linkages increases, while the number of J_4 linkages decreases. Hence, the Fe cations segregate in small clusters, without long-range order.

Al/Fe/Mg = 2/1/1

This composition can be found in natural and synthetic smectites. This system is quite different from those discussed above, in that the heat capacity anomaly (Fig. 10a) is quite broad and occurs at a fairly low temperature. The structure is shown in Figure 10b, together with the partial ordering plots in Figures 10c–10e. From these figures it can be seen that there is a fairly high degree of short-range order, but no long-range order. Fe atoms cluster together to a certain extent, while nearest-neighbor Mg-Mg interactions are avoided. The ordered configuration of this sample shows that the Fe atoms segregate in very small clusters that are smaller than in the previous sample with Al/Fe/Mg = 3/1/2. Similar behavior was found in the samples with Al/Fe/Mg = 4/1/1 and 7/2/3, although the size of Fe clusters is smaller than in 2/1/1.

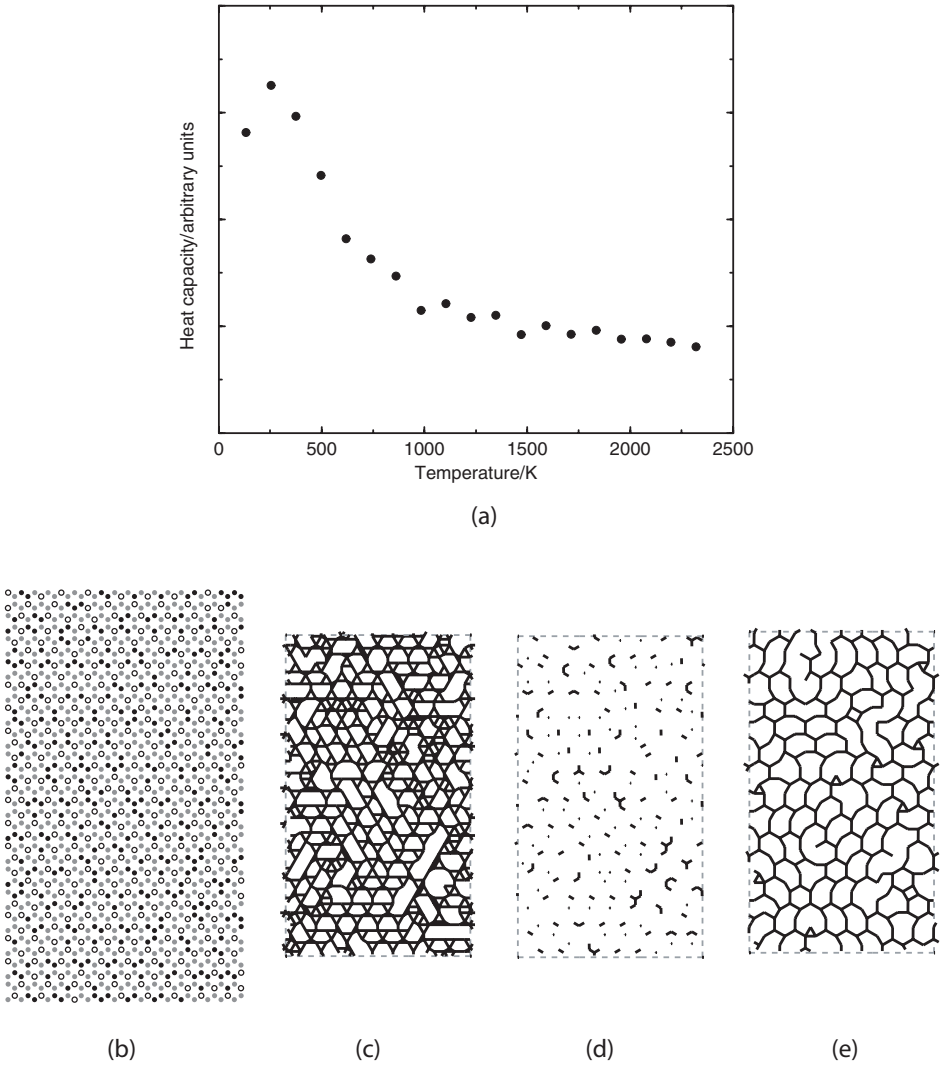

FIGURE 10. Results for Al/Fe/Mg = 2/1/1. (**a**) Heat capacity data. (**b**) Low temperature snapshot. Grey circles indicate Al, black circles Fe, and open circles Mg. (**c**) Partial ordering pattern for Al. (**d**) Partial ordering pattern for Fe. (**e**) Partial ordering pattern for Mg.

DISCUSSION

By considering all the systems presented above, together with those from Sainz-Díaz et al. (2003b), we can make several observations about the most ordered configuration of each system (whether it exhibits short- or long-range order). It seems that in all cases ordering is dominated by the large size of the Mg-Mg J_1; that is, Mg atoms are always dispersed with respect to each other. Similarly, Fe atoms tend to form either clusters or chains, and it seems that the behavior of Al atoms simply changes to accommodate the behavior of the Fe and Mg atoms. This clustering behavior of Fe is also observed in experiments (Besson et al. 1987; Drits et al. 1997; Cuadros et al. 1999).

For compositions close to nontronite, the Fe cation forms globular clusters with no connections between the clusters. This fact agrees with experimental results (Manceau et al. 2000), where small Fe domains separated by Al and Mg were found in nontronites. The lack of connections between Fe clusters is consistent with experimental results for nontronites (Lear and Stucki 1990), who showed that a lack of magnetic ordering was observed at low temperatures. However, when the Al content is higher, although still lower than the Fe content, the Fe clustering forms long chains of Fe atoms along the octahedral sheet, suggesting high probabilities of magnetic conductivity. This fact can be very interesting for the experimentalists who synthesize dioctahedral clays with the aim of producing materials with magnetic properties. It is likely that the special zone around 2/3/1 and 3/2/1 Al/Fe/Mg compositions can be useful for synthesizing new dioctahedral clays with magnetic properties, although the small crystal sizes and layer disorder could be a handicap in this respect.

In the Al-rich samples, short-range ordering is observed for Fe, in that it forms small clusters. This is consistent with previous experimental studies on illites and smectites that came to the

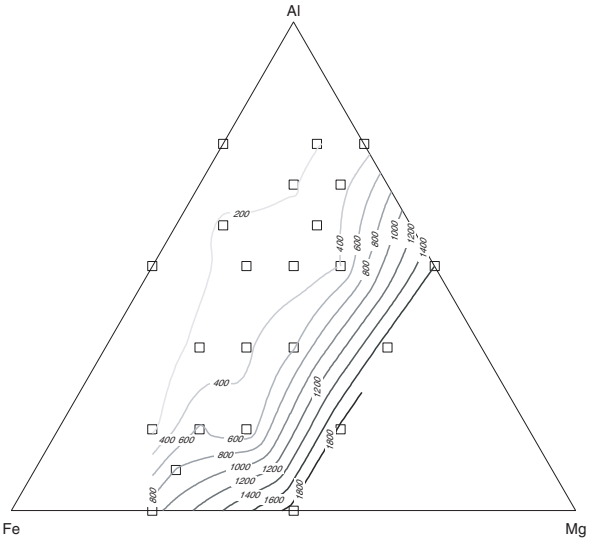

FIGURE 11. Contour plot showing phase transition temperatures (or heat capacity anomaly temperatures in systems without a phase transition) for all compositions studied.

same conclusion (Cuadros et al. 1999; Sainz-Díaz et al. 2001a); when the Mg content increases, the Fe segregation decreases.

PHASE TRANSITIONS

Figure 11 shows a contour plot of the transition temperatures in systems that exhibit long-range order at low temperature, and in addition the temperatures at which other heat capacity anomalies occur in systems that exhibit short-range order at low temperature.

It is interesting to observe that the only compositions in which full long-range order occurs are the two-species systems and the Al/Fe/Mg 1/1/1 mixture. Other systems exsolve at low temperature into a mixture of phases (e.g., Al/Fe/Mg 3/1/2), or simply show short-range order by forming chains or clusters of atoms (e.g., Al/Fe/Mg 2/3/1, 2/1/1). It is possibly easier for long-range order to occur in systems where the ratios of atoms to one another are simple.

In general, the transition temperatures (or heat capacity anomaly temperatures if there is no phase transition) decrease as the amount of Mg decreases and the amount of Al increases. This is not surprising in view of the relative values of the *J*s. In the two-species systems (Table 1), the largest *J*s are for the Al/Mg system, followed by the Fe/Mg system. Since Mg features in both systems with high *J*s, it follows that it should have a greater influence on the temperatures, followed by Al, which is the other member of the system with the highest *J* values.

An interesting effect visible from Figure 11 is that of dilution; that is, the decrease in transition temperature with decreasing proportion of one cation. This has been documented for Al/Si ordering in a variety of systems (Dove et al. 1996; Myers et al. 1998), and it can be observed for all three of the binary systems studied here—for example, the transition temperature in Fe/Mg = 3/1 is much lower than that in Fe/Mg = 1/1.

Another interesting feature is that the naturally occurring compositions all have low transition temperatures/heat capacity anomaly temperatures. This fact can be explained from the *J* values. These samples have greater proportions of Fe and Al than Mg. Hence, the ordering phase transitions will be controlled more by the *J*s of Fe and Al cations that are much lower than the Mg ones (Table 2).

The results presented in this work show that the cation ordering is highly dependent on the relative cation composition in these three-species systems. In general a segregation tendency of Fe and dispersion tendency of Mg is observed. In samples with a high Fe content, the Fe atom forms globular clusters with low Al content samples, whereas when the Al content is significant the Fe cations form linear clusters.

The good agreement with experiment found in this work can validate this theoretical approach as a useful tool for experimentalists to predict cation ordering with respect to the cation composition in synthesis of clay minerals.

ACKNOWLEDGMENTS

The authors are grateful for the financial support of NERC (M.T. Dove), EPSRC (E.J. Palin), exchange program Royal Society of UK/CSIC of Spain (C.I. Sainz-Díaz), and BTE2000-1146-CO2-01 MCYT project (A. Hernández-Laguna). The Monte Carlo simulations were performed on the Mineral Physics Group's Beowulf cluster at the Department of Earth Sciences, University of Cambridge, and on the University of Cambridge's High Performance Computing Facility.

REFERENCES CITED

Besson, G., Drits, V.A., Daynyak, L.G., and Smoliar, B.B. (1987) Analysis of cation distribution in dioctahedral micaceous minerals on the basis of IR spectroscopy data. Clay Minerals, 22, 465–478.

Bosenick, A., Dove, M.T., Myers, E.R., Palin, E.J., Sainz-Díaz, C.I., Guiton, B., Warren, M.C., Craig, M.S., and Redfern, S.A.T. (2001) Computational methods for the study of energies of cation distributions: applications to cation-ordering phase transitions and solid solutions. Mineralogical Magazine, 65, 193–219.

Bush, T.S., Gale, J.D., Catlow, C.R.A., and Battle, P.D. (1994) Self-consistent interatomic potentials for the simulation of binary and ternary oxides. Journal of Materials Chemistry, 4, 831–837.

Cuadros, J., Sainz-Díaz, C.I., Ramírez, R., and Hernández-Laguna, A. (1999) Analysis of Fe segregation in the octahedral sheet of bentonitic illite-smectite by means of FT-IR, ^{27}Al MAS NMR and reverse Monte Carlo simulations. American Journal of Science, 299, 289–308.

Dove, M.T., Thayaparam, S., Heine, V., and Hammonds, K.D. (1996) The phenomenon of low Al-Si ordering temperatures in aluminosilicate framework structures. American Mineralogist, 81, 349–362.

Drits, V.A., Dainyak, L.G., Muller, F., Besson, G., and Manceau, A. (1997) Isomorphous cation distribution in celadonites, glauconites and Fe-illites determined by infrared, Mössbauer and EXAFS spectroscopies. Clay Minerals, 32, 153–179.

Gale, J.D. (1997) GULP: a computer program for the symmetry-adapted simulation of solids. Journal of the Chemical Society: Faraday Transactions, 93, 629–637.

Grauby, O., Petit, S., and Decarreau, A. (1991) Distribution of Al-Fe-Mg in octahedral sheets of synthetic smectites : Study of three binary solid-solutions. Proceedings of the 7th EUROCLAY Conference, 441–446.

Güven, N. (1988) Smectites. In S.W. Bailey, Ed., Hydrous Phyllosilicates (exclusive of micas), Reviews in Mineralogy, 19, p. 497–559. Mineralogical Society of America, Washington, D.C.

Lear, P.R. and Stucki, J.W. (1990) Magnetic properties and site occupancy of iron in nontronite. Clay Minerals, 25, 3–14.

Manceau, A., Lanson, B., Drits, V.A., Chateigner, D., Gates, W.P., Wu, J., Huo, D., and Stucki, J.W. (2000) Oxidation-reduction mechanism of iron in dioctahedral smectites: I. Crystal chemistry of oxidized reference nontronites. American Mineralogist, 85, 133–152.

Muller, F., Besson, G., Manceau, A., and Drits, V.A. (1997) Distribution of isomorphous cations within octahedral sheets in montmorillonite from Camp-Bertaux. Physics and Chemistry of Minerals, 24, 159–166.

Myers, E.R., Heine, V., and Dove, M.T. (1998) Thermodynamics of Al/Al avoidance in the ordering of Al/Si tetrahedral framework structures. Physics and Chemistry of Minerals, 25, 457–464.

Palin, E.J., Dove, M.T., Redfern, S.A.T., Bosenick, A., Sainz-Díaz, C.I., and Warren, M.C. (2001) Computational study of tetrahedral Al-Si ordering in muscovite. Physics and Chemistry of Minerals, 28, 534–544.

Palin, E.J., Dove, M.T., Redfern, S.A.T., and Sainz-Díaz, C.I. (2003) Computational

study of tetrahedral Al-Si and octahedral Al-Mg ordering in phengite. Physics and Chemistry of Minerals, 30, 293–304

Sainz-Díaz, C.I., Cuadros, J., and Hernández-Laguna, A. (2001a) Cation distribution in the octahedral sheet of dioctahedral 2:1 phyllosilicates by using inverse Monte Carlo methods. Physics and Chemistry of Minerals, 28, 445–454.

Sainz-Díaz, C.I., Hernández-Laguna, A., and Dove, M.T. (2001b) Modelling of dioctahedral 2:1 phyllosilicates by means of transferable empirical potentials. Physics and Chemistry of Minerals, 28, 130–141.

Sainz-Díaz, C.I., Palin, E.J., Hernández-Laguna, A., and Dove, M.T. (2003a) Octahedral cation ordering of illite and smectite. Theoretical exchange potential determination and Monte Carlo simulations. Physics and Chemistry of Minerals, 30. 382–392.

Sainz-Díaz, C.I., Palin, E.J., Dove, M.T., and Hernández-Laguna, A. (2003b) Ordering of Al, Fe and Mg cations in the octahedral sheet of smectites and illites by means of Monte Carlo simulations. American Mineralogist, 88, 1033–1045.

Schröder, K.-P., Sauer, J., Leslie, M., Catlow, C.R.A., and Thomas, J.M. (1992) Bridging hydroxyl groups in zeolitic catalysts: a computer simulation of their structure, vibrational properties and acidity in protonated faujasites (H–Y zeolites). Chemical Physics Letters, 188, 320–325.

Schroeder, P.A. (1993) A chemical, XRD, and ^{27}Al MAS NMR investigation of Miocene Gulf Coast shales with application to understanding illite-smectite crystal-chemistry. Clays and Clay Minerals, 41, 668–679.

Warren, M.C., Dove, M.T., Myers, E.R., Bosenick, A., Palin, E.J., Sainz-Díaz, C.I., Guiton, B., and Redfern, S.A.T. (2001) Monte Carlo methods for the study of cation ordering in minerals. Mineralogical Magazine, 65, 221–248.

Winkler, B., Dove, M.T., and Leslie, M. (1991) Static lattice energy minimization and lattice dynamics calculations on aluminosilicate minerals. American Mineralogist, 76, 313–331.

MANUSCRIPT RECEIVED JANUARY 30, 2003
MANUSCRIPT ACCEPTED MAY 6, 2003
MANUSCRIPT HANDLED BY MARIA BRIGATTI

APPENDIX 1. EMPIRICAL INTERATOMIC POTENTIALS

The model interatomic potentials used to parameterize the systems under investigation in this work are given here. Further discussions of the method are given in Sainz-Díaz et al. (2003a, 2003b).

In the following formulae, we use the following general symbols: E to represent energy, r to represent an interatomic distance, and θ to represent an angle between two interatomic vectors. A zero subscript indicates an equilibrium value. All ions are modeled using formal charges except the hydroxyl ions, although the charges on the hydroxyl groups still sum to the formal value of $-1e$.

Short-range Si-O, Al-O, K-O, and O-O interactions are modeled by Buckingham energy potentials:

$$E = A\exp(-r/\rho) - Cr^{-6}$$

For Al-O and K-O, C has zero value. O-Si-O tetrahedral and O-Al-O tetrahedral and octahedral interactions are modeled by three-body potentials:

$$E = \frac{1}{2}k\left(\theta - \theta_0\right)^2 \quad (A.2)$$

O-H interactions within the hydroxyl groups are modeled by a Morse potential:

$$E = D\left[\left(1 - \exp\left[-a\left(r - r_0\right)\right]\right)^2 - 1\right] \quad (A.3)$$

All O atoms except those forming part of the hydroxyl groups are modeled by the shell model, where atoms are considered to consist of a core comprising the nucleus and tightly bound inner electrons, surrounded by a massless shell of outer electrons. The cores are assigned a charge of $+0.86902e$ and the shells a charge of $-2.86902e$, maintaining the formal value for the overall charge of $-2e$. The core and shell are held together by a harmonic core-shell interaction:

$$E = \frac{1}{2}Kd^2 \quad (A.4)$$

where d is the core-shell separation.

APPENDIX TABLE 1A. Parameter values used in interatomic potentials, the equations for which are given in Equations A.1–A.4 (see footnotes in Appendix Table 1c)

Potential type	Parameter values			Reference*
Buckingham†	*A* (eV)	r (Å)	*C* (eV.Å^{-6})	
Si^{4+}–O^{2-}	1283.9073	0.3205	10.6616	1
Si^{4+}–$O^{1.426-}$	999.98	0.3012	0.0	1
Al^{3+}–$O^{1.426-}$	1142.6775	0.2991	0.0	2
Al^{3+}–O^{2-}	1460.3	0.2991	0.0	1
(Fe^{3+}–O^{2-})‡	3219.335	0.2641	0.0	3
Mg^{2+}–$O^{1.426-}$	1142.6775	0.2945	0.0	1
Mg^{2+}–O^{2-}	1428.5	0.2945	0.0	1
K^{+}–O^{2-}	65269.71	0.2130	0.0	1
Na^{+}–O^{2-}	1271.504	0.3000	0.0	3
Mg^{2+}(interlayer)–O^{2-}	946.627	0.31813	0.0	4
Ca^{2+}–O^{2-}	2272.74	0.2986	0.0	3
O^{2-}–O^{2-}	22764.0	0.149	27.88	1
$H^{0.426+}$–O^{2-}	325.0	0.25	0.0	1

APPENDIX TABLE 1B. Parameter values used in interatomic potentials, the equations for which are given in Equations A.1–A.4 (see footnotes in Appendix Table 1c)

Potential type	Parameter values				Reference*
	D (eV)	*a* (Å^{-1})	r_o (Å)	*K* (eV.Å^{-2})	
Morse§:					
$H^{0.426+}$–$O^{1.426-}$	7.0525	2.1986	0.9485		1
Core–shell:					
$O_{core}^{0.86902-}$–$O_{shell}^{2.86902-}$				74.92	1

APPENDIX TABLE 1C. Parameter values used in interatomic potentials, the equations for which are given in Equations A.1–A.4

Potential type	Parameter values		Reference*
Three-body:	*k* (eV.rad^{-2})	θ_0 (°)	
O^{2-}–Si^{4+}–O^{2-}	2.09724	109.47	1
(O^{2-}–Al^{3+}(T)–O^{2-}) ‖	2.09724	109.47	1
(O^{2-}–M(Oc)–O^{2-}) ‖	2.09724	90	1
(O^{2-}M(Oc)–$O^{1.426-}$) ‖	2.09724	90	
$O^{1.426-}$–M(Oc)–$O^{1.426-}$ ‖	2.09724	90	

* References: 1 = Winkler et al. (1991), 2 = Schröder et al. (1992), 3 = Bush et al. (1994), 4 = Gale (1997).
† Parameters for Buckingham potentials between cation cores and O atom shells. When $C = 0$, the function takes the form of a Born-Mayer potential. All cutoffs at 12 Å.
‡ With O_{shell}^{2-} or $O_{core}^{1.426-}$.
§ Modified Morse potential between cores.
‖ T in the tetrahedral sheet; Oc in octahedral coordination, M any cation in the octahedral sheet (Al^{3+}, Fe^{3+}, Mg^{2+}).